nature communications

Article

https://doi.org/10.1038/s41467-025-62846-z

Neural Network Nodal Ambient Noise Tomography of a transient plumbing system under unrest, Vulcano, Italy

Received: 19 July 2024

Accepted: 31 July 2025

Published online: 27 August 2025

Check for updates

Douglas Sami Stumpp[1], Iván Cabrera-Pérez[1], Geneviève Savard[1], Tullio Ricci[2], Mimmo Palano[3,4], Salvatore Alparone[4], Andrea Ursino[4], Federica Sparacino[4], Anthony Finizola[5,6], Francisco Muñoz Burbano[1], María-Paz Reyes Hardy[1], Joël Ruch[1], Costanza Bonadonna[1] & Matteo Lupi[1]

Volcanic risk escalates significantly during unrest. In late 2021, the Italian island of Vulcano entered into a phase of unrest featuring Very Long Period seismic events, which are considered to be markers of magma and gas flowing across the volcanic plumbing system. Here we show how Neural Network Nodal Ambient Noise Tomography generates a high-resolution shear-wave velocity model for investigating the causative drivers of Vulcano's unrest. Using a deep learning model we harvest seismic dispersion data from a dense nodal seismic network deployed during the early unrest's phase. The inverted 3-D model reveals a high-resolution tomography of the shallow part of a volcanic system in unrest. If deployed and rapidly processed in (near) real-time during periods of unrest, Neural Network Nodal Ambient Noise Tomography can lead to dynamic and adaptive evacuation plans. Such advances would contribute to more effective, source-dependent risk mitigation schemes in volcanic regions, potentially saving lives.

The island of Vulcano, along with Lipari and Salina, constitutes the central volcanic ridge of the Aeolian archipelago on the Tyrrhenian Sea, southern Italy (Fig. 1A). This central sector is aligned with the NNW-SSE regional Aeolian-Tindari-Letojanni (ATLF) strike-slip fault system[1–4] (Fig. 1A–B). Vulcano experienced multiple Vulcanian-style eruptions with frequent transitions from magmatic to phreatomagmatic activity[5], and has remained quiescent since its last eruption in 1888 - 1890 AD. However, below La Fossa caldera (Fig. 1C), the primary volcanic feature of Vulcano, an active hydrothermal system at a depth of between 0.5 and 1 km below sea level (b.s.l.)[6–8] has been intermittently affected by episodic inputs of magmatic fluids and volcanic degassing unrest over the past four decades[9,10]. Considering the increase in population of Vulcano during the summer season and the importance of the island for tourists, the exposure to volcanic hazards remains exceedingly high even for minor eruptive events or episodes of increased degassing[3,11,12].

Since early September 2021, La Fossa caldera exhibited increased activity characterized by a rapid intensification of previously unseen unrest indicators[8,12–16]. This activity was marked by a large rate of increase in fumarolic temperatures, accompanied by substantial emissions of (CO_2-rich and SO_2) magmatic gases and diffuse soil fluxes[8,10,13,14,16]. A centimeter-scale uplift was also observed at La Fossa, along with a significant increase of local seismicity, and the detection of Very Long Period (VLP) seismic signals[8,14–16]. VLPs are a distinctive feature of this unrest as they are usually attributed to the release of magma and/or pressurized magmatic fluids through the shallow

[1]Department of Earth Sciences, University of Geneva, Geneva, Switzerland. [2]Istituto Nazionale di Geofisica e Vulcanologia, Sezione Roma 1, Italy. [3]Dipartimento di Scienze della Terra e del Mare, Università degli Studi di Palermo, Palermo, Italy. [4]Istituto Nazionale di Geofisica e Vulcanologia, Osservatorio Etneo, Sezione di Catania, Italy. [5]Université de La Réunion, Laboratoire GéoSciences Réunion, F-97744 Saint Denis, France. [6]Université de Paris, Institut de Physique du Globe de Paris, CNRS, F-75005 Paris, France. e-mail: douglas.stumpp@unige.ch; matteo.lupi@unige.ch

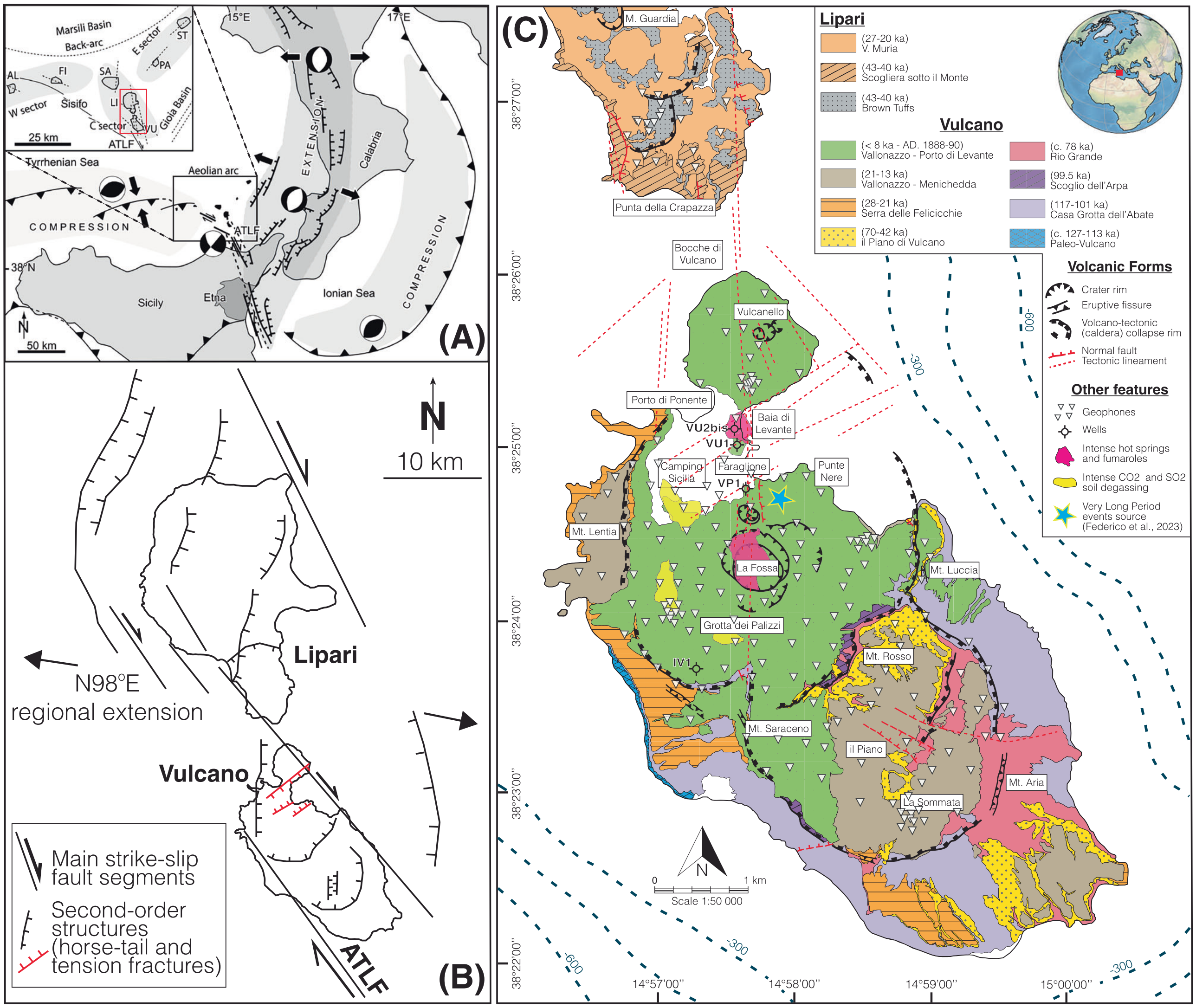

Fig. 1 | Maps of the structural and geological context in the Aeolian Archipelago. (**A**) Regional simplified structural map and location of the three main sectors of the Aeolian volcanic arc. AL: Alicudi, FI: Filicudi, SA: Salina, LI: Lipari, VU: Vulcano, PA: Panarea, ST: Stromboli, ATLF: Aeolian-Tindari-Letojanni Fault system (reproduced from previous authors[77] with permission. ©2016. American Geophysical Union.). The red box is shown in panel (**B**) Cinematic model of the transtensional ATLF and resulting structural pull-apart ("*en échelon*") configuration along the Lipari-Vulcano Complex (LVC) (redrawn from previous authors[2,62,81]). Majority of the red secondary antithetic faults are highlighted in panel (**C**) Geological map of Vulcano and southern Lipari with morphostructural features (redrawn from previous authors[3,4,77,82]). The white triangles show the location of the geophones. Additional features (wells, fumaroles, degassing areas, Very Long Period events source) highlighted by previous studies[12,14,57,58] are shown in accordance with the legend.

fractured volcanic conduits[12,14,16–18]. Although the unrest phase is no longer at its peak, and the yellow alert level declared by the Italian Civil Protection on October 1st 2021 was set back to green on December 19th 2023[19], an increase in VLP events, fumaroles temperatures and gas emissions was detected again starting from May 2024[20]. The current unrest shares similarities with Vulcano's previous crisis of the late 1970s to early 1990s[16], suggesting that the current episode may continue for several more years[21].

The latest conceptual models discussing this unrest suggest either the persistent degassing, at a reduced rate, of a deep-seated magmatic source at about 4 - 5 km depth[8], or increased activity of the shallow hydrothermal system[16,21]. In the past, some authors proposed the replenishment of the shallow hydrothermal system with magmatic fluids originating from the pulsating degassing process of a deeper, pressurized, and stationary magmatic body[5,7–9,11–14,22,23]. Nonetheless, Vulcano's plumbing system is believed to be a polybaric intricate magmatic network with reservoirs having sill and dike-like structures[8,11,22]. Unfortunately, geophysical data are sparse and mainly constrained by airborne geophysics[24–27]. Onshore studies do not penetrate enough in the plumbing system to reveal the interplay between magmatic and hydrothermal fluids[28–30]. Only recent investigations have shown the plumbing system down to a few kilometers depth but none of them had enough resolution to distinguish between the magmatic and the hydrothermal system[12,31]. The recent development of nodal technologies allows the investigation of highly scattering systems with a great resolution[32–34]. To understand what may have driven the 2021 Vulcano unrest, we deployed a nodal network of 196 sensors across Vulcano and Lipari islands (Fig. 1C).

In this work, we harness the capabilities of a deep neural network to facilitate the automatic and rapid recovery of extensive seismic dispersion data, conducting a Neural Network Nodal Ambient Noise Tomography (N^3ANT) of Vulcano. This endeavor aims to investigate the seismic S-wave velocity structure of a volcanic system under unrest, with the objective of understanding its nature and improving the volcanic hazard assessment in the region. Our findings reveal how

https://doi.org/10.1038/s41467-025-62846-z

tectonic and volcanic processes interact and suggest that fault dynamics may trigger volcanic unrest.

Results and discussion

We present the 3-D S-wave velocity model of Vulcano retrieved from the N^3ANT workflow. As detailed in the Supplementary Methods, N^3ANT leverages a deep neural network to harvest nodal array dispersion data from depth-sensitive Rayleigh waves, which dominate virtual seismograms estimated from ambient noise cross-correlation. These data are inverted using a two-step inversion scheme to retrieve the 3-D S-wave velocity model. This involves nonlinear 2-D travel-time tomography inversions[35] that are followed by a trans-dimensional Markov chain Monte Carlo (McMC) probabilistic search algorithm[36] for 1-D depth inversions. The 3-D S-wave velocity model is shown by means of horizontal (Fig. 2) and vertical (Figs. 3–4) sections. The traces of the vertical sections are indicated in Fig. 2A, and the main anomalies are distinguished between high (H) and low (L) velocity anomalies. A detailed interpretation of each anomaly mentioned below is provided in the Supplementary Discussion and summarized in the Supplementary Table 1. Additionally, the 3-D S-wave velocity model is shown by mean of the Supplementary Movie 1.

Ray-path density maps (Supplementary Fig. 1), combined with a noise directivity analysis (Supplementary Fig. 2A), synthetic resolution tests (Supplementary Figs. 3–6) and a depth-sensitivity analysis (Supplementary Fig. 14), demonstrate the capacity of our network configuration to retrieve reliable information up to 2 km depth. Maximum resolution is reached within the upper first kilometer, below which it starts to decrease and becomes poor below 2 km. Note that the lower resolution achieved in the northern parts of the model allows to spatially detect the anomalies, but prevents the systematic resolution of their precise geometry. For sake of clarity and to avoid drawing interpretations on poorly resolved areas, we combine ray-path density (Supplementary Fig. 1), synthetic tests (Supplementary Figs. 3–6), and depth-sensitivity (Supplementary Fig. 14) information to remove parts of the 3-D model in our illustrations (Supplementary Methods section).

The S-wave velocity model of Vulcano shows La Fossa surrounded in all azimuths by low-velocity zones (L3 in Figs. 2A–B, 3, and 4) that largely fill the caldera between 0 and ~1 km b.s.l., and extend towards the northwest and southeast of the velocity model. These anomalies are overlying and connected to NE-striking, sub-vertical, low-velocity regions (L2 in Figs. 2C–E, 3, and 4), which originate from the bottom of the velocity model at 2 km b.s.l. and are located below the northwestern and southeastern extremities of La Fossa cone. High-velocity anomalies (H2 and H3 in Figs. 2, 3, and 4) are observed from near-surface to greater depths along the rims of La Fossa caldera, respectively located along the eastern (il Piano - Mt. Rosso - Mt. Lucia) and western (Mt. Saraceno - Mt. Lentia - Porto di Ponente) rim. At greater depths, between 1 and 2 km b.s.l., a large and elongated high-velocity region (H1 in Figs. 2C–E, 3, and 4) is observed centered below La Fossa cone. This anomaly appears to be connected to H2 and to H3, respectively below the eastern and western rim of La Fossa caldera (Figs. 2C–E and 3A,C,E). However, the sub-vertical L2 regions (Figs. 2C–E, 3A,B,D, and 4) seem to interrupt these connections, effectively offsetting this large high-velocity domain (H1 + H2 + H3) into distinct anomalies. One high-velocity anomaly (H4 in Figs. 2C–E and 4) is observed below the southernmost part of Lipari, between 1 and 2 km b.s.l. This anomaly is offset from those below Vulcano by a noticeably large sub-vertical low-velocity region (L1 in Figs. 2, 3A, and 4), which, like the L2 anomalies, originates from the bottom of the velocity model at 2 km b.s.l. and is located below the Bocche di Vulcano region between Lipari and Vulcanello.

The velocity of seismic shear waves is sensitive to several physical attributes such as, among others, stress conditions, porosity, permeability, and pore fluid content, which in turn strongly depend on water saturation, temperature and confining pressure[37–40]. While the elastic properties of rocks hosting active hydrothermal systems differ from unaltered conditions[16], fractured and fluid-saturated regions exhibit lower S-wave velocities (V_S)[37,41–43] compared to their intact protoliths. Volcanoes with low V_S usually reflect the presence of (mixed sea/meteoric, magmatic brines and/or hydrothermal) fluid-filled pores and/or partial melts[37–40,44–46], as well as fractured units and unconsolidated shallow volcanoclastic deposits[40,44,46–48]. In short, discriminating among the physical state of fluids solely based on V_S is non-unique and statements would be speculative, which applies to the proposed interpretation.

The N^3ANT model is in agreement with previous local earthquake tomographies[31,49] (LET) acquired at Vulcano and neighboring regions. At the regional scale, the V_S model supports the separation of Vulcano into two distinct regions, namely the southern high and northern low V_S sectors[49]. At the local scale, this separation remains consistent but disagreement is observed at shallow depths (<1 km). The central portion of La Fossa cone and Vulcanello are marked by low V_S (L3 anomalies in Figs. 2A–B and 3), where the local scale LET features high P-wave velocity (V_P) anomalies[31]. Discrepancies between N^3ANT and LET models lie in the parameterization of the inverse problem and the type of wave energy (surface and body waves, respectively) employed for the tomography. Nonetheless, N^3ANT offers higher lateral resolution than LET at shallow depths due to the dense ray-path coverage of surface waves (Supplementary Fig. 1) made possible by the large number of stations and the homogeneous distribution of noise sources (Supplementary Fig. 2A). In addition, our acquisition occurred during a volcanic unrest, when increased advective fluid flow characterizes the upper portion of the volcanic edifice. The combination of rising fluids (which condense and percolate through the cone) and hydrothermal circulation of sea and meteoric waters through the loose and permeable infills of La Fossa is expected to lower V_S beneath the volcanic structure. In fact, time-lapse tomography studies have shown the highly transient nature of plumbing systems[50], which justifies the differences observed from tomographies decades apart.

Further comparisons can be drawn from a magnetotelluric (MT) model[12] acquired during our experiment. The MT model reveals an elongated resistive structure below La Fossa surrounded by shallow conductive zones. This aligns with the V_S model, which shows a system articulated by a broad low-velocity domain within La Fossa caldera, overlaying a large high-velocity region culminating at ~1 km depth (L3, and H1–3 anomalies in Figs. 2A–B and 3A–C and E). The presence of cooled magmatic intrusions is often interpreted from high seismic velocities[51] coinciding with high resistivity[40,52–54], while seismic velocities in association with high conductivity suggest fracturing along with (hydrothermal) fluid circulation and alteration[47,55,56].

Observations made by geothermal exploration wells (Fig. 1C) also strongly support our V_S model. For instance, the L2 and L3 anomalies located on Baia di Levante marks the hydrothermal alteration and hot steam discharges at shallow depths (~ 200°C at ~ 200 m b.s.l.) evidenced by the VU1 and $VU2_{bis}$ wells[57–59]. The Vulcano Porto well (VP1) indicates a convection-conduction transition boundary (between shallow permeable rocks and deep impermeable lavas) at ~ 600 m b.s.l., and sub-volcanic bodies at the maximum depth of 1'000 m[12,58]. While the transition boundary remains undetected due to the strong low-velocity intensity of the L2 and L3 anomalies, the 1 km deep sub-horizontal roof delineated by the observed high-velocity anomalies (Figs. 3 and 4) fits the first occurrence of intrusive bodies seen in the well. This further aligns and is supported by ~ 300 concurrent VLP events, which remained spatially quasi-stationary throughout their monitoring period[14]. The average VLP hypocenter has a depth of ~0.85 ± 0.23 km b.s.l.[14], which falls at the L2–L3 anomalies' interface (Figs. 3A and 4). The Isola di Vulcano well (IV1) penetrated a monzodioritic intrusion at 1.36 km depth[60], which was also detected by the

https://doi.org/10.1038/s41467-025-62846-z

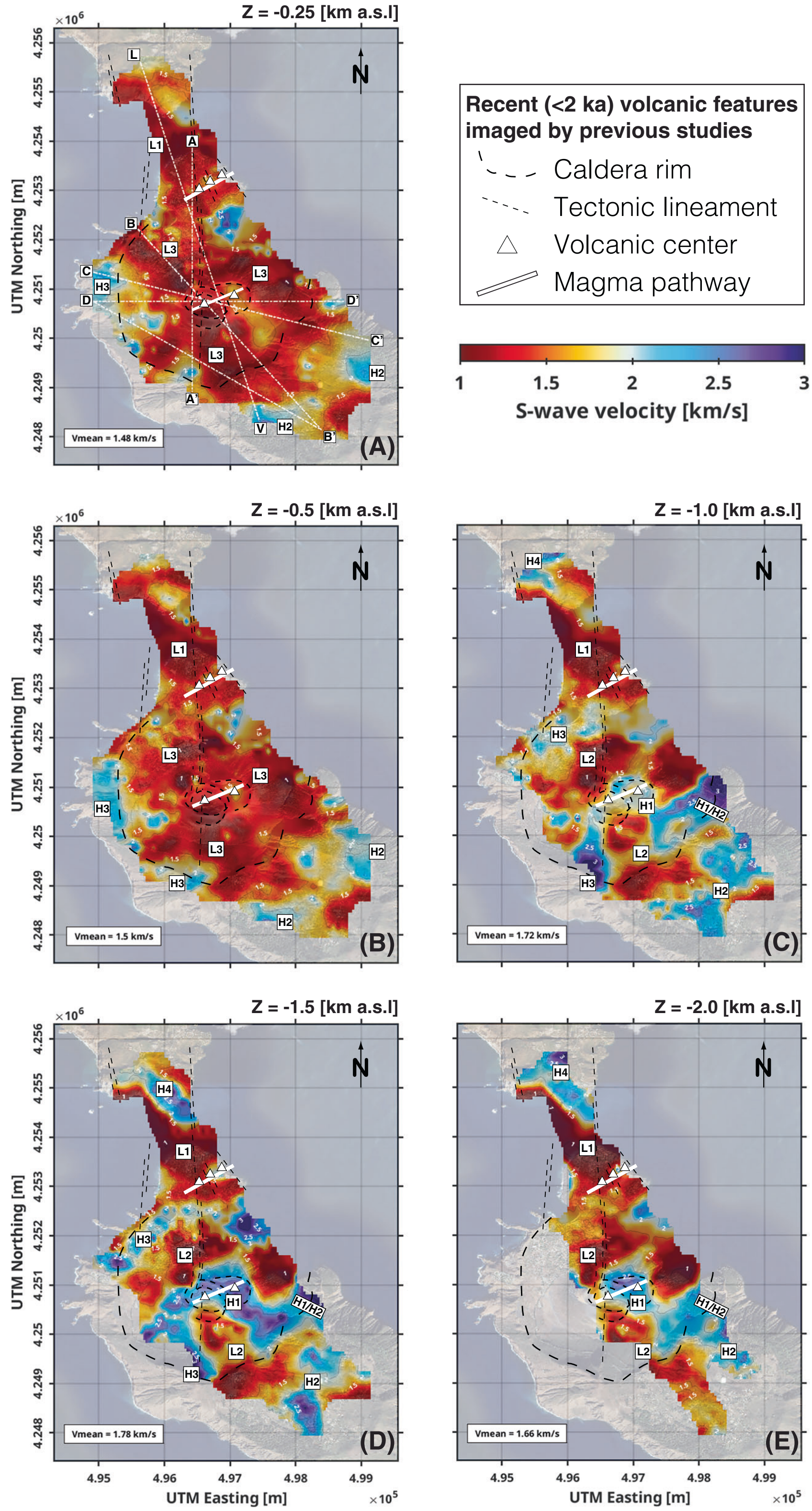

Fig. 2 | S-wave velocity maps at different depths. Horizontal maps are shown in panels (**A**), (**B**), (**C**), (**D**), and (**E**). The white dotted lines shown in (**A**) correspond to the vertical cross-sections shown in Figs. 3 and 4. The literature-suggested caldera rims and magmato-tectonic lineaments that controlled the recent (<2 ka) eruptive history of the Lipari-Vulcano Complex are shown by the black-dotted lines (adapted from previous authors[77] with permission. ©2016. American Geophysical Union.). The white triangles show, from north to south, the alignment of the volcanic centers of Vulcanello and La Fossa, respectively. The main anomalies are named and distinguished between high (H) and low (L) velocity anomalies. The model is cropped with respect to ray-path density, synthetic tests, and depth-sensitivity information (Supplementary Methods and Figs. 1, 3–6, 14), as resolution starts to decrease below 1 km b.s.l. The satellite background map comes from Google Earth[83].

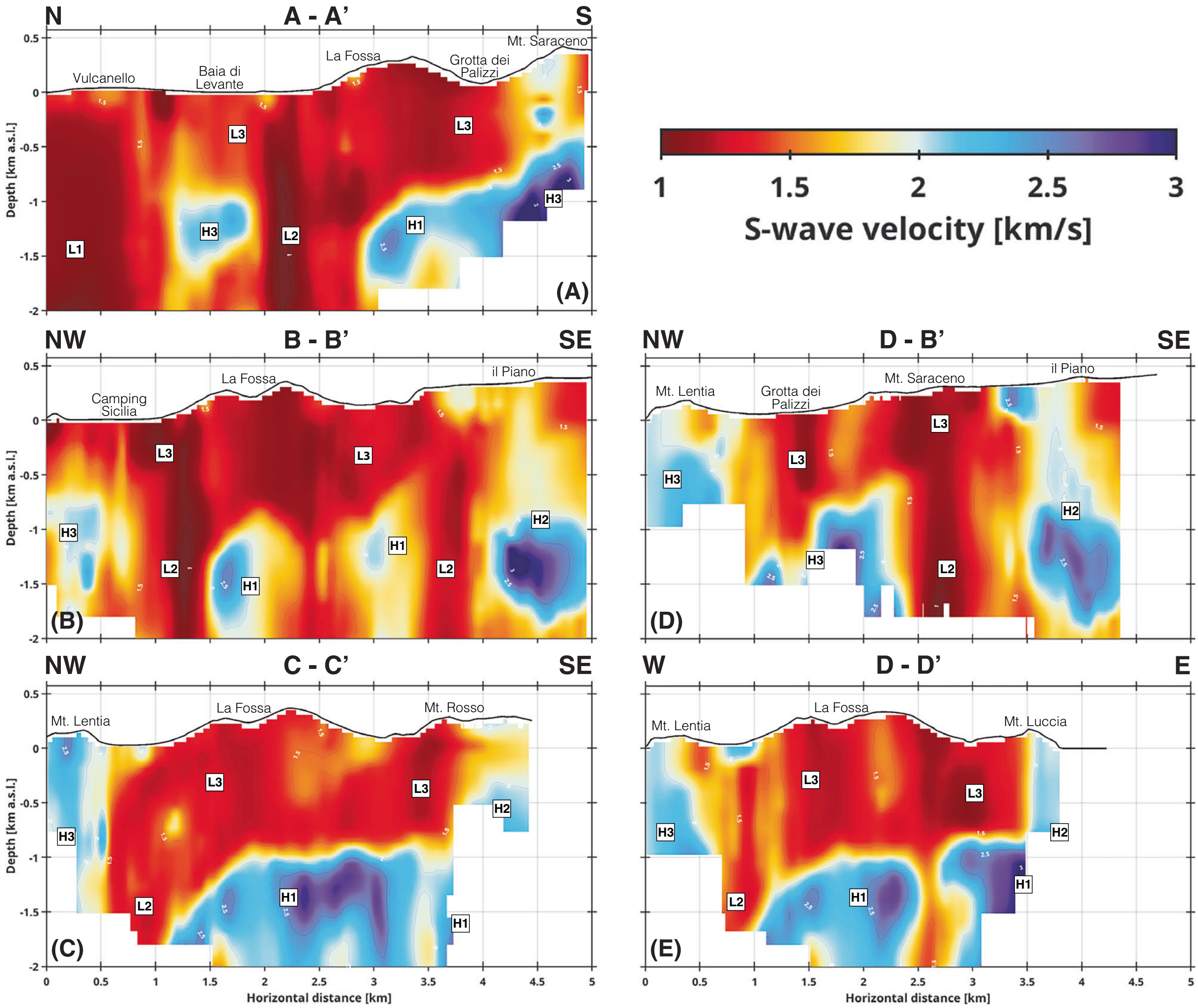

Fig. 3 | Vertical sections of the S-wave velocity model. The vertical sections are shown in panels (**A**), (**B**), (**C**), (**D**), and (**E**), and their traces are indicated in Fig. 2A. The main anomalies are named and distinguished between high (H) and low (L) velocity anomalies. The model is cropped with respect to ray-path density, synthetic tests, and depth-sensitivity information (Supplementary Methods and Figs. 1, 3–6, 14), as resolution starts to decrease below 1 km b.s.l. The Digital Elevation Model comes from Sonny's LiDAR DTMs database (https://sonny.4lima.de/).

local-scale LET[31]. The H3 anomaly fits the detection of this intrusion below Grotta dei Palizzi (Fig. 3D).

Figure 4 shows the conceptual model we propose for the shallow plumbing system of Vulcano superimposed on a vertical section of the S-wave velocity 3-D model. This section is sub-parallel to the ATLF and connects the southernmost part of Lipari to il Piano across the sites of Vucanello, Baia di Levante, and La Fossa. All anomalies mentioned above are shown, as well as the locations of key wells[57,58] and the average VLP hypocenter[14]. Our model does not require the shallow emplacement of new batches of magma, although we cannot exclude the occurrence of ancient melts ponding at shallow depths[22,61]. For instance, the L1 and L2 anomalies show V_S values as low as 1 km s^{-1}, which may be compatible with melts (e.g., magma, mush, etc.). However, they are also compatible with a fluid-rich and highly fractured region or with a more ductile rheology, such as a crystallizing domain where fluids are not as mobile as in a freshly emplaced melt.

We propose a key role of local tectonics in driving unrest and argue, in agreement with previous authors, that the ATLF is a right-lateral NW-striking transtensional fault along which the Vulcano-Lipari-Salina volcanism develops[1,2,4,62]. The transtension causes an "*en échelon*" configuration (Fig. 1B) and the formation of local pull-apart basins that are controlled by primary NW-striking strike-slip and second-order antithetic N- to NE-striking faults[1–4,62]. The secondary NE-striking faults act as weak zones along which major eruptive center alignments develop[63,64] (white lines and triangles in Fig. 2) and contribute to the northwestward opening of the system from extension[1,4,65,66]. Clear examples of such NE-striking normal faults can be observed in Fig. 2C–D, where the transition between the fast and slow V_S anomalies depicts well-defined NE-striking structures extending along the complete island (from il Piano to Porto di Ponente). A closer observation highlights that such structures affect the whole plumbing system of Vulcano (black normal faults in Fig. 4). This localized extension facilitates the upwelling of dikes, fluids and supercritical brines, ultimately leading to a northward increase in volcanic activity. The progressive normal-fault driven sliding of the northern sector of Vulcano's edifice is also in agreement with the development of the hydrothermal field north of La Fossa. Shallow earthquakes (e.g., less than 2 km depth) accommodating extension and pull-apart basin formation do not necessarily have to be characterized by large magnitudes, as deformation is lubricated by the vigorous fluid flow of the region.

Our conceptual volcano-tectonic model of Vulcano finds similarities with flank-instability models proposed for other volcanic settings

 https://doi.org/10.1038/s41467-025-62846-z

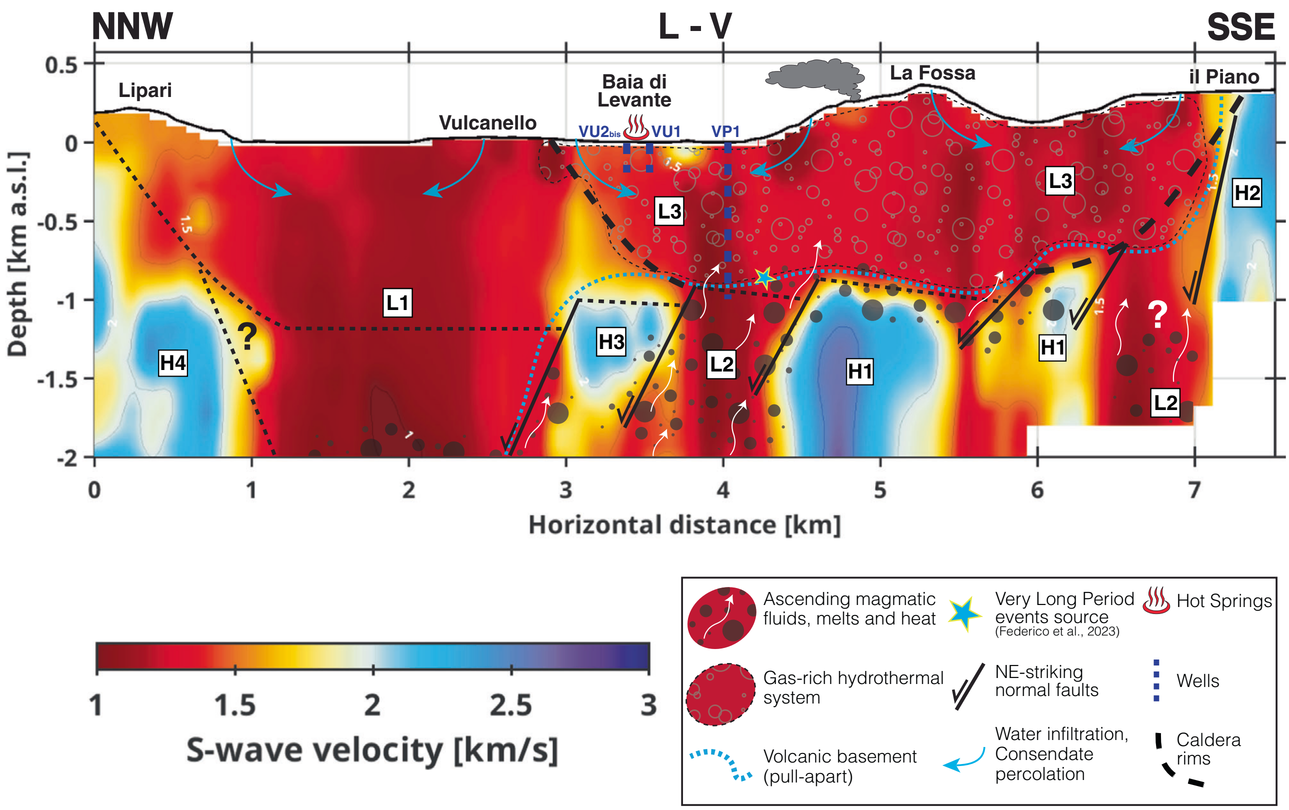

Fig. 4 | Conceptual volcano-tectonic model. Vertical section of the S-wave velocity model, sub-parallel to the Aeolian-Tindari-Letojanni fault system, between Lipari and the volcanic vents of Vulcano. The trace of the vertical section is indicated in Fig. 2A. The main anomalies are named and distinguished between high (H) and low (L) velocity anomalies. Interpretive elements are superimposed on the model, such as: the pulled-apart volcanic basement (H1, H2, H3) affected by NE-striking normal faults which release magmatic fluids/melts into the potential (L2) reservoir(s) and feeding-system(s). These fluids/melts migrate along these sub-vertical structures towards the active hydrothermal system (L3), as evidenced by the summit fumaroles, the coastal hot springs, and the Very Long Period events[14] (blue star). The model is cropped with respect to ray-path density, synthetic tests, and depth-sensitivity information (Supplementary Methods and Figs. 1, 3–6, 14), as resolution starts to decrease below 1 km b.s.l. The Digital Elevation Model comes from Sonny's LiDAR DTMs database (https://sonny.4lima.de/).

(e.g., La Soufrière, Guadeloupe[67,68] and Mt. Etna, Italy[69]), where the repetitive unrest episodes induce long-term motion and destabilization of La Fossa's northern flank. However, the corollary of tectonically-driven volcanism implies that even minor perturbations may affect the delicate equilibrium of the plumbing system of Vulcano, ultimately promoting unrest. Such unrest would, therefore, not necessarily be caused by the emplacement of magma at shallow depths but may be driven by any geological process capable of affecting the baric equilibrium of the plumbing system of Vulcano. This could be the replenishment of magma at greater depths but also the tectonic activation of the normal faults shown in Fig. 4. Such lubricated faults may be easily perturbed because of the near-critical state of the upper volcanic edifice[70]. In this context, the VLPs identified in the 2021 unrest may simply be caused by the mobilization of brines promoted by tectonic activity or magma emplacement at greater depths[71].

The N^{3}ANT model that we propose introduces inversion imaging of the shallow plumbing system of a volcano in unrest. Such a model may be routinely acquired to monitor the evolution of the plumbing system over time. Temporal variations may occur, pointing out regions undergoing changes that may be interpreted by including complementary datasets (e.g., magnetotelluric-seismic clustering[52], ambient noise attenuation[72,73], P-wave[74,75], and joint Rayleigh/Love group and phase velocity[76] tomography). The northern low-V_S L2 domain underlies the region where the largest deformation occurred during the 2021 unrest of Vulcano. Our study is an encouraging starting point to begin monitoring volcanic crises with tomographic neural network-driven seismic acquisitions capable of delivering reliable and rapid inversions that can drive risk mitigation plans during unrest.

Our 3-D S-wave velocity model of Vulcano shows an image of its plumbing system during the 2021 unrest and helps to assess the causative drivers of the volcanic crisis. The V_S model reveals the occurrence of an extensional setting where the right-lateral transtension of the Aeolian-Tindari-Letojanni Fault system creates local extensional structures. Such pull-apart basins are controlled by NE-striking secondary faults along which fluids rise, driven by the high geothermal gradient of the region caused by magma emplacement at depth. We do not identify any newly emplaced magmatic body between Lipari and Vulcano in the first two kilometers of the crust. However, we identify regions that could host cooling melts ponding at the base of the hydrothermal system. We propose that such regions could be interpreted as old degassing melts that, if perturbed by an external source such as a tectonic earthquake for instance, could release gas and brines. The rise of such a mix could cause the Very Long Period (VLP) events recorded during the last unrest.

Our study highlights the interplay between tectonic and volcanic activity and suggests that volcanic unrest may be driven by fault activity. If perturbed, faults affecting the plumbing systems of volcanoes may help release the fluids trapped at depth and lead to the observations recorded at Vulcano since 2021. Our velocity model is supported by previous geophysical observations and borehole data and represents a unique example of a tomography acquired during volcanic unrest. Today deep neural networks facilitate the rapid processing of large datasets paving the ground to time-lapse tomographic acquisitions. This could be introduced in early warning systems to support the management of volcanic crises.

Data availability

The empirical Green's functions, the Rayleigh waves dispersion curves and group velocity maps, and the S-wave velocity model data[78] generated in this study are available at https://zenodo.org/records/15789417. The data analysis and results supporting the findings of this study are provided in the Supplementary Information and Supplementary Movie 1.

Code availability

Dispersion curves were measured using the open-source Matlab software EGFAnalysisTimeFreq (Yao et al., 2011[79], https://github.com/ShaoboYang-USTC/EGFAnalysisTimeFreq), combined with the open-source Convolutional Neural Network DisperPicker (Yang et al., 2022[80], https://github.com/ShaoboYang-USTC/DisperPicker). 2-D travel-time tomography inversions were performed using the nonlinear scheme of Cabrera-Pérez et al., 2021[35]. 1-D Depth inversions were performed using the open-source software BayHunter (Dreiling and Tilmann, 2019[36], https://github.com/jenndrei/BayHunter).

References

1. Ventura, G. Tectonics, structural evolution and caldera formation on Vulcano Island (Aeolian Archipelago, southern Tyrrhenian Sea. *J. Volcanol. Geotherm. Res.* **60**, 207–224 (1994).
2. Ventura, G., Vilardo, G., Milano, G. & Pino, N. A. Relationships among crustal structure, volcanism and strike–slip tectonics in the Lipari–Vulcano Volcanic Complex (Aeolian Islands, Southern Tyrrhenian Sea, Italy). *Phys. Earth Planet. Inter.* **116**, 31–52 (1999).
3. De Astis, G. et al. Chapter 11 Geology, volcanic history and petrology of Vulcano (central Aeolian archipelago). *Geol. Soc., Lond., Mem.* **37**, 281–349 (2013).
4. Barreca, G. et al. New insights in the geodynamics of the Lipari–Vulcano area (Aeolian Archipelago, southern Italy) from geological, geodetic and seismological data. *J. Geodyn.* **82**, 150–167 (2014).
5. Alparone, S. et al. Time-space variation of volcano-seismic events at La Fossa (Vulcano, Aeolian Islands, Italy): new insights into seismic sources in a hydrothermal system. *Bull. Volcanol.* **72**, 803–816 (2010).
6. Chiodini, G. et al. Geochemical and seismological investigations at Vulcano (Aeolian Islands) during 1978–1989. *J. Geophys. Res.* **971**, 11025–11032 (1992).
7. Cannata, A. et al. Multiparametric Approach in Investigating Volcano-Hydrothermal Systems: the Case Study of Vulcano (Aeolian Islands, Italy). *Pure Appl. Geophys.* **169**, 167–182 (2012).
8. Aiuppa, A. et al. Mafic magma feeds degassing unrest at Vulcano Island, Italy. *Commun. Earth Environ.* **3**, 1–15 (2022).
9. Granieri, D. et al. Correlated increase in CO2 fumarolic content and diffuse emission from La Fossa crater (Vulcano, Italy): Evidence of volcanic unrest or increasing gas release from a stationary deep magma body? *Geophys. Res. Lett.* **33**, L13316 (2006).
10. Inguaggiato, S. et al. The Extensive Parameters as a Tool to Monitoring the Volcanic Activity: The Case Study of Vulcano Island (Italy). *Remote Sens* **14**, 1283 (2022).
11. Selva, J. et al. Multiple hazards and paths to eruptions: a review of the volcanic system of Vulcano (Aeolian Islands, Italy). *Earth Sci. Rev.* **207**, 103186 (2020).
12. Di Giuseppe, M. G., Isaia, R. & Troiano, A. Three-dimensional magnetotelluric modeling of Vulcano Island (Eolie, Italy) and its implications for understanding recent volcanic unrest. *Sci. Rep.* **13**, 16458 (2023).
13. Inguaggiato, S. et al. The volcanic activity changes occurred in the 2021–2022 at Vulcano island (Italy), inferred the abrupt variations of soil CO2 output. *Sci. Rep.* **12**, 21166 (2022).
14. Federico, C. et al. Inferences on the 2021 Ongoing Volcanic Unrest at Vulcano Island (Italy) through a Comprehensive Multidisciplinary Surveillance Network. *Remote Sens.* **15**, 1405 (2023).
15. Stissi, S. C., Currenti, G., Cannavò, F. & Napoli, R. Evidence of poroelastic inflation at the onset of the 2021 Vulcano Island (Italy) unrest. *Front. Earth Sci.* **11**, 1179095 (2023).
16. Di Traglia, F. et al. Multi-Temporal InSAR, GNSS and Seismic Measurements Reveal the Origin of the 2021 Vulcano Island (Italy) Unrest. *Geophys. Res. Lett.* **50**, e2023GL104952 (2023).
17. Chouet, B. A. & Matoza, R. S. A multi-decadal view of seismic methods for detecting precursors of magma movement and eruption. *J. Volcanol. Geotherm. Res.* **252**, 108–175 (2013).
18. McNutt, S. R. & Roman, D. C. Chapter 59 - Volcanic Seismicity. In *The Encyclopedia of Volcanoes (Second Edition)* (ed. Sigurdsson, H.) 1011–1034. https://doi.org/10.1016/B978-0-12-385938-9.00059-6 (Amsterdam: Academic Press, 2015).
19. Presidenza del Consiglio dei Ministri. *Dipartimento della Protezione Civile*. Vulcano. https://rischi.protezionecivile.gov.it/en/volcanic/volcanoes-italy/vulcano/ (2025).
20. Istituto Nazionale di Geofisica e Vulcanologia. *Sezioni di Catania e Palermo Vulcano, Bollettino Mensile del Giugno 2024*. https://cme.ingv.it/bollettini-e-comunicati/bollettini-ingv-vulcano/2356-20240702-bollettino-mensile-vulcano/file (2024).
21. Pailot-Bonnétat, S. et al. Anatomy of thermal unrest at a hydrothermal system: case study of the 2021–2022 crisis at Vulcano. *Earth, Planets, and Space* **75**, 159 (2023).
22. Peccerillo, A., Frezzotti, M. L., De Astis, G. & Guido, V. Modeling the magma plumbing system of Vulcano (Aeolian Islands, Italy) by integrated fluid-inclusion geobarometry, petrology, and geophysics. *Geology* **34**, 17–20 (2006).
23. Ricci, T. et al. Hydrothermal fluid flow disruptions evidenced by subsurface changes in heat transfer modality: The La Fossa cone of Vulcano (Italy) case study. *Geology* **43**, 959–962 (2015).
24. Supper, R., De Ritis, R., Motschka, K. & Chiappini, M. Aeromagnetic anomaly images of Vulcano and Southern Lipari Islands (Aeolian Archipelago, Italy). *Ann. Geophys.* **47**, 1803–1810 (2004).
25. De Ritis, R., Blanco-Montenegro, I., Ventura, G. & Chiappini, M. Aeromagnetic data provide new insights on the volcanism and tectonics of Vulcano Island and offshore areas (southern Tyrrhenian Sea, Italy). *Geophys. Res. Lett.* **32**, 2–5 (2005).
26. Okuma, S. et al. Shallow Subsurface Structure of the Vulcano-Lipari Volcanic Complex, Italy, Constrained by Helicopter-Borne Aeromagnetic Surveys. *Explor. Geophys.* **37**, 129–138 (2006).
27. Blanco-Montenegro, I., De Ritis, R. & Chiappini, M. Imaging and modelling the subsurface structure of volcanic calderas with high-resolution aeromagnetic data at Vulcano (Aeolian Islands, Italy). *Bull. Volcanol.* **69**, 643–659 (2007).
28. Revil, A. et al. Inner structure of La Fossa di Vulcano (Vulcano Island, southern Tyrrhenian Sea, Italy) revealed by high-resolution electric resistivity tomography coupled with self-potential, temperature, and CO2 diffuse degassing measurements. *J. Geophys. Res. Solid Earth* **113**, B07207 (2008).
29. Bruno, P. P. G. & Castiello, A. High-resolution onshore seismic imaging of complex volcanic structures: An example from Vulcano Island, Italy. *J. Geophys. Res. Solid Earth* **114**, B12 (2009).
30. Barde-Cabusson, S. et al. New geological insights and structural control on fluid circulation in La Fossa cone (Vulcano, Aeolian Islands, Italy). *J. Volcanol. Geotherm. Res.* **185**, 231–245 (2009).
31. Chiarabba, C., Pino, N., Guido, V. & Vilardo, G. Structural features of the shallow plumbing system of Vulcano Island Italy. *Bull. Volcanol.* **66**, 477–484 (2004).
32. Hand, E. A boom in boomless seismology. *Science* **345**, 720–721 (2014).
33. Obermann, A. et al. Combined Large-N Seismic Arrays and DAS Fiber Optic Cables across the Hengill Geothermal Field, Iceland. *Seismol. Res. Lett.* **93**, 2498–2514 (2022).
34. Wu, S.-M. et al. Crustal Characterization of the Hengill Geothermal Fields: Insights From Isotropic and Anisotropic Seismic Noise

Imaging Using a 500-Node Array. *J. Geophys. Res. Solid Earth* **129**, e2024JB028915 (2024).
35. Cabrera-Pérez, I. et al. A nonlinear multiscale inversion approach for ambient noise tomography. *Geophys. J. Int.* **225**, 1158–1173 (2021).
36. Dreiling, J. & Tilmann, F. BayHunter - McMC transdimensional Bayesian inversion of receiver functions and surface wave dispersion. GFZ Data Services. *GFZ Data Services* https://doi.org/10.5880/GFZ.2.4.2019.001 (2019).
37. Nakajima, J. & Hasegawa, A. Tomographic imaging of seismic velocity structure in and around the Onikobe volcanic area, northeastern Japan: implications for fluid distribution. *J. Volcanol. Geotherm. Res.* **127**, 1–18 (2003).
38. Vanorio, T., Virieux, J., Capuano, P. & Russo, G. Three-dimensional seismic tomography from P wave and S wave microearthquake travel times and rock physics characterization of the Campi Flegrei Caldera. *J. Geophys. Res. Solid Earth* **110**, B03201 (2005).
39. Lesage, P., Heap, M. J. & Kushnir, A. A generic model for the shallow velocity structure of volcanoes. *J. Volcanol. Geotherm. Res.* **356**, 114–126 (2018).
40. Ulberg, C. W. et al. Local Source Vp and Vs Tomography in the Mount St. Helens Region With the iMUSH Broadband Array. *Geochem., Geophys., Geosyst.* **21**, e2019GC008888 (2020).
41. Lees, J. M. Seismic tomography of magmatic systems. *J. Volcanol. Geotherm. Res.* **167**, 37–56 (2007).
42. Yukutake, Y., Honda, R., Harada, M., Arai, R. & Matsubara, M. A magma-hydrothermal system beneath Hakone volcano, central Japan, revealed by highly resolved velocity structures. *J. Geophys. Res. Solid Earth* **120**, 3293–3308 (2015).
43. Austria, D. C. & Benson, P. M. Fracture, fluid and saturation effects on the seismic attributes of rocks from the Southern Negros geothermal field, Philippines. *J. Volcanol. Geotherm. Res.* **408**, 107099 (2020).
44. Paulatto, M. et al. Magma chamber properties from integrated seismic tomography and thermal modeling at Montserrat. *Geochem., Geophys., Geosyst.* **13**, Q01014 (2012).
45. Okada, T. et al. Seismic velocity structure in and around the Naruko volcano, NE Japan, and its implications for volcanic and seismic activities. *Earth, Planets and Space* **66**, 114 (2014).
46. Obermann, A., Lupi, M., Mordret, A., Jakobsdóttir, S. S. & Miller, S. A. 3D-ambient noise Rayleigh wave tomography of Snæfellsjökull volcano, Iceland. *J. Volcanol. Geotherm. Res.* **317**, 42–52 (2016).
47. Di Stefano, R. & Chiarabba, C. Active source tomography at Mt. Vesuvius: Constraints for the magmatic system. *J. Geophys. Res. Solid Earth* **107**, ESE 4–1–ESE 4–15 (2002).
48. Calò, M., Di Luccio, F., Persaud, P. & Ventura, G. Ambient Noise Tomography of the Lipari Volcanic Island (Southern Italy) From a Dense Nodal Array. *Geophys. Res. Lett.* **50**, e2022GL101022 (2023).
49. Totaro, C. et al. New insights on the active degassing system of the Lipari–Vulcano complex (South Italy) inferred from Local Earthquake Tomography. *Sci. Rep.* **12**, 18867 (2022).
50. Vargas, C. A. et al. Breathing of the Nevado del Ruiz volcano reservoir, Colombia, inferred from repeated seismic tomography. *Sci. Rep.* **7**, 46094 (2017).
51. Brenguier, F., Shapiro, N. M., Campillo, M., Nercessian, A. & Ferrazzini, V. 3-D surface wave tomography of the Piton de la Fournaise volcano using seismic noise correlations. *Geophys. Res. Lett.* **34**, 2305 (2007).
52. García-Yeguas, A. et al. A 3D joint interpretation of magnetotelluric and seismic tomographic models: The case of the volcanic island of Tenerife. *Comput. Geosci.* **109**, 95–105 (2017).
53. Bedrosian, P. A., Peacock, J. R., Bowles-Martinez, E., Schultz, A. & Hill, G. J. Crustal inheritance and a top-down control on arc magmatism at Mount St Helens. *Nat. Geosci.* **11**, 865–870 (2018).
54. Cabrera-Pérez, I. et al. Geothermal and structural features of La Palma island (Canary Islands) imaged by ambient noise tomography. *Sci. Rep.* **13**, 12892 (2023).
55. Cordell, D. et al. Integrating Magnetotelluric and Seismic Images of Silicic Magma Systems: A Case Study From the Laguna del Maule Volcanic Field, Central Chile. *J. Geophys. Res. Solid Earth* **125**, e2020JB020459 (2020).
56. Cabrera-Pérez, I. et al. Ambient noise tomography of Gran Canaria island (Canary Islands) for geothermal exploration. *Geothermics* **108**, 102609 (2023).
57. Sommaruga, C. Le ricerche geotermiche svolte a Vulcano negli anni '50. *Rendiconti della Soc.à Ital. di Mineralogia e Petrologia* **39**, 355–366 (1984).
58. Todesco, M. Modeling of the geothermal activity at Vulcano (Aeolian Islands, Italy). In *Proceedings of the World Geothermal Congress '95* 1309–1314 (Firenze: International Geothermal Association, 1995).
59. Fulignati, P., Gioncada, A. & Sbrana, A. Geologic model of the magmatic-hydrothermal system of Vulcano (Aeolian Islands, Italy). *Mineral. Petrol.* **62**, 195–222 (1998).
60. Faraone, D., Silvano, A. & Verdiani, G. The monzogabbroic intrusion in the island of Vulcano, Aeolian Archipelago, Italy. *Bull. Volcanol.* **48**, 299–307 (1986).
61. Clocchiatti, R. et al. Assessment of a shallow magmatic system: the 1888–90 eruption, Vulcano Island, Italy. *Bull. Volcanol.* **56**, 466–486 (1994).
62. Mazzuoli, R., Tortorici, L. & Ventura, G. Oblique rifting in Salina, Lipari and Vulcano islands (Aeolian islands, southern Italy). *Terra Nova* **7**, 444–452 (1995).
63. Gabbianelli, G. Submarine morphology and tectonics of Vulcano (Aeolian Islands, Southern Tyrrhenian Sea). *Acta Vulcanol* **1**, 135–141 (1991).
64. Gambino, S., Milluzzo, V., Scaltrito, A. & Scarfì, L. Relocation and focal mechanisms of earthquakes in the south-central sector of the Aeolian Archipelago: New structural and volcanological insights. *Tectonophysics* **524–525**, 108–115 (2012).
65. Giocanda, A. La Fossa caldera, Vulcano: inferences from deep drillings. *Acta Vulcanol*. **1**, 115–125 (1991).
66. Mattia, M. et al. Tectonic features of the Lipari-Vulcano complex (Aeolian archipelago, Italy) from 10 years (1996–2006) of GPS data. *Terra Nova* **20**, 370 (2008).
67. Rosas-Carbajal, M., Komorowski, J.-C., Nicollin, F. & Gibert, D. Volcano electrical tomography unveils edifice collapse hazard linked to hydrothermal system structure and dynamics. *Sci. Rep.* **6**, 29899 (2016).
68. Heap, M. J. et al. Alteration-Induced Volcano Instability at La Soufrière de Guadeloupe (Eastern Caribbean). *J. Geophys. Res. Solid Earth* **126**, e2021JB022514 (2021).
69. Nicolosi, I., Caracciolo, F. D. 'A., Branca, S., Ventura, G. & Chiappini, M. Volcanic conduit migration over a basement landslide at Mount Etna (Italy). *Sci. Rep.* **4**, 5293 (2014).
70. Heap, M. J. et al. Hydrothermal alteration can result in pore pressurization and volcano instability. *Geology* **49**, 1348–1352 (2021).
71. Lupi, M. et al. Non-eruptive unrest and the role of magmatic brines, Vulcano, Italy. *Copernicus Meeting (EGU24-21336)*. https://doi.org/10.5194/egusphere-egu24-21336 (2024).
72. Borleanu, F. et al. Seismic attenuation tomography of Eastern Europe from ambient seismic noise analysis. *Geophys. J. Int.* **236**, 547–564 (2024).
73. Cabrera-Pérez, I. et al. 3-D intrinsic attenuation tomography using ambient seismic noise applied to La Palma Island (Canary Islands). *Sci. Rep.* **14**, 27354 (2024).
74. Nakata, N., Chang, J. P., Lawrence, J. F. & Boué, P. Body wave extraction and tomography at Long Beach, California, with ambient-

noise interferometry. *J. Geophys. Res. Solid Earth* **120**, 1159–1173 (2015).
75. Riahi, A., Shomali, Z.-H., Obermann, A. & Kamayestani, A. 3-D body-wave tomography from the seismic ambient noise recorded by a dense array in the Dehdasht area, Iran. *Geophys. J. Int.* **234**, 1332–1341 (2023).
76. Lee, S.-J., Kim, S., Rhie, J., Kang, T.-S. & Kim, Y. Upper crustal shear wave velocity and radial anisotropy beneath Jeju Island volcanoes from ambient noise tomography. *Geophys. J. Int.* **225**, 1332–1348 (2021).
77. Ruch, J., Vezzoli, L., De Rosa, R., Di Lorenzo, R. & Acocella, V. Magmatic control along a strike-slip volcanic arc: The central Aeolian arc (Italy). *Tectonics* **35**, 407–424 (2016).
78. Stumpp, D. S. et al. Neural Network Nodal Ambient Noise Tomography of a transient plumbing system under unrest, Vulcano, Italy [Data set]. *Zenodo* https://doi.org/10.5281/zenodo.15789417 (2025).
79. Yao, H., Gouédard, P., Collins, J. A., McGuire, J. J. & Van Der Hilst, R. D. Structure of young East Pacific Rise lithosphere from ambient noise correlation analysis of fundamental- and higher-mode Scholte-Rayleigh waves. *Comptes Rendus Geosci*. **343**, 571–583 (2011).
80. Yang, S. et al. Automatically Extracting Surface-Wave Group and Phase Velocity Dispersion Curves from Dispersion Spectrograms Using a Convolutional Neural Network. *Seismol. Res. Lett.* **93**, 1549–1563 (2022).
81. Gioncada, A., Mazzuoli, R., Bisson, M. & Pareschi, M. T. Petrology of volcanic products younger than 42 ka on the Lipari–Vulcano complex (Aeolian Islands, Italy): an example of volcanism controlled by tectonics. *J. Volcanol. Geotherm. Res.* **122**, 191–220 (2003).
82. Forni, F. et al. Chapter 10 Stratigraphy and geological evolution of the Lipari volcanic complex (central Aeolian archipelago). *Geol. Soc., Lond. Mem.* **37**, 213–279 (2013).
83. Google Google Earth Pro V 7.3.6.10201. (December 14, 2015). *Vulcano island, Italy. 38 24 18.01N, 14 57 45.08E, Eye alt 10.5 km. SIO, NOAA, U.S. Navy, NGA, GEBCO, Airbus 2025*. https://earth.google.com/web/ (2015).

Acknowledgements

This work was possible thanks to the special collaboration with the Istituto Nazionale di Geofisica e Vulcanologia (INGV), whose Dipartimento Vulcani, Osservatorio Etneo and Centro Monitoraggio Eolie, provided the logistical support for the N^{3}ANT activities during the 2021 unrest at Vulcano, with the help of Lucia Pruiti (INGV). T.R. was partially supported by funding of the "Accordo Quadro tra il Dipartimento della Protezione Civile e l'Istituto Nazionale di Geofisica et Vulcanologia 2022-2025". The contents of this article represent the authors' ideas and do not necessarily correspond to the official opinion and policies of the Dipartimento della Protezione Civile - Presidenza del Consiglio dei Ministri. M.-P.R.H. and C.B. were supported by the SNSF project (grant number 200020_188757). M.L. and D.S.S. are supported for the investigation of high enthalpy geothermal systems by the SNSF project MIGRATE - A Multidisciplinary and InteGRated Approach for geoThermal Exploration (grant number 209434). The computations were performed at the University of Geneva using Yggdrasil HPC service. Figures. 1A and 2 are reproduced and adapted from Ruch et al., 2016[77], with permission from John Wiley and Sons. ©2016. American Geophysical Union.

Author contributions

D.S.S. led the study, performed the data analysis, bridged the N^{3}ANT workflow and performed the inversions, with assistance from G.S. and I.C-P. M.L. and C.B. conceived the experiment and organized the logistics with T.R. M.L. and G.S. organized the nodal network field campaign and contributed to raw data processing. G.S., T.R., S.A., A.U., M.P., F.S., F.M.-B., M.-P.R.H., and M.L. participated in data collection in the field. J.R. and A.F. contributed actively to the geological conceptual model discussion. All the authors reviewed the manuscript and contributed to the interpretation and discussion.

Competing interests

The authors declare no competing interests.

Additional information

Supplementary information The online version contains supplementary material available at https://doi.org/10.1038/s41467-025-62846-z.

Correspondence and requests for materials should be addressed to Douglas Sami Stumpp or Matteo Lupi.

Peer review information *Nature Communications* thanks Luca De Siena, who co-reviewed with Fabrizio Magrini, Pilar Sánchez-Pastor and the other, anonymous, reviewer(s) for their contribution to the peer review of this work. A peer review file is available.